Effects of Fully Ionised Dusty Plasma on the Polarization Properties of Obliquely Incident Electromagnetic Waves

Liping Gan (甘利萍)[1,†], Zilin Wang (王紫琳)[1], Lixin Guo (郭立新)[2]，Haichao Zhan (詹海潮)[1]，Hao Du (杜浩)[1]

[1] *School of Optoelectronic Engineering, Henan Normal University, Xinxiang, 453007, China*

[2] *School of Physics, Xidian University, Xi'an, 710071, China*

This study investigated the effects of fully ionised dusty plasma on the polarization properties of obliquely incident electromagnetic (EM) waves. First, a complex permittivity model of fully ionised dusty plasma was established based on the Fokker–Planck–Landau collision model and orbit motion limited theory. Then, taking X-band right-handed circularly polarised waves as an example, the axial ratio, phase difference, and polarization mismatch loss were obtained using the equivalent transmission line method when the EM waves were obliquely incident on the fully ionised dusty plasma. Numerical results indicated that increasing the incident angle aggravated the polarization mismatch, and polarization reversal occurred at large incident angles. Appropriately increasing the dust radius or dust density increased the critical angle of polarization reversal and decreased the polarization mismatch loss. It is worth noting that the dust radius had the greatest effect. In addition, increasing the incident frequency within the X-band slightly intensified the polarization mismatch. The results of this study provide an important theoretical basis for the polarization matching design of reentry communication links and blackout mitigation.

Keywords: electromagnetic (EM) wave propagation, plasma sheath, fully ionised dusty plasma, polarization properties

PACS: 52.40.Kh, 94.30.Tz, 52.40.Dd

1. Introduction

When a hypersonic vehicle enters the Earth's atmosphere, a plasma sheath forms on the surface of the vehicle as a result of severe friction with the surrounding air [1]. This plasma sheath can cause significant attenuation of radar signals and lead to communication blackouts [2,3]. Compared with ordinary plasma, the plasma sheath is a complex dusty plasma containing ablated particles. The collision and charging effects between these dust and charged particles significantly alter the electromagnetic properties of the medium, which may be one of the most important reasons for the communication blackout [4–7].

Numerous studies have been conducted on the interaction between dusty plasma and electromagnetic (EM) waves. Jia et al. [8] analysed the attenuation characteristics of EM waves in fully ionised dusty plasma based on the Bhatnagar–Gross–Krook (BGK) collision model. However, the BGK model is inherently better suited for short-range collisions and exhibits limited accuracy in describing long-range Coulomb collisions. Liu et al. [9] compared the attenuation characteristics of the left-handed circularly polarised (LHCP) and right-handed circularly polarised (RHCP) components of terahertz waves in inhomogeneous dusty plasma. Their results showed that a strong external magnetic field creates a low-absorption band in the attenuation of RHCP terahertz waves. Dan et al. [10] introduced the Fokker–Planck–Landau (FPL) collision model and verified its applicability in fully ionised plasma regimes. Guerra et al. [11] developed a Mie–Debye scattering model to investigate the effects of the dust radius

† Corresponding author. E-mail: ganliping@htu.edu.cn

and charge number on the scattering cross section. They found that Mie scattering dominates at short wavelengths, whereas Debye scattering prevails at long wavelengths, with both the dust particle size and charge state determining the magnitude of the scattering cross section. Chen et al. [12] derived a finite-difference time-domain iterative formulation for inhomogeneous fully ionised dusty plasma based on the FPL model, and analysed the influence of dust parameters on the radar cross sections of targets. Their numerical results demonstrated that increasing the dust radius weakens the Debye shielding effect and increases the radar cross section of the target, which is also strongly influenced by plasma collision and dust charging effects.

However, previous studies have mainly focused on the amplitude attenuation, transmission coefficients, reflection coefficients, and scattering characteristics of EM waves. In addition to attenuating the signal amplitude, the plasma sheath also alters the polarization state of EM waves, resulting in a polarization mismatch loss between the transmitted wave and receiving antenna. This polarization mismatch loss is also a critical source of the signal degradation that occurs during the blackout phenomenon [13–15]. Shahrokhi et al. [16] studied the polarization evolution process of EM waves in motional plasma and proposed a novel plasma diagnostic method. Bai et al. [17] systematically analysed the polarization evolution of obliquely incident EM waves in plasma using the transmission line analogy method, but the influences of ablated dust particles were not taken into account. Our group [18] investigated the effects of weakly ionised dusty plasma on the polarization properties of obliquely incident EM waves. The results indicated that dust particles can alleviate polarization deterioration and reduce the polarization mismatch loss. To date, no systematic study has clearly revealed the effects of dust particles in the fully ionised state on the polarization characteristics of obliquely incident EM waves.

This study theoretically investigated the polarization state of transmitted waves passing through fully ionised dusty plasma. The axial ratio, phase difference, and polarization mismatch loss of the transmitted waves were obtained. Numerical results indicated that the dust radius had the most significant effect. The results can provide a theoretical basis for the polarization matching design of reentry communication links and blackout mitigation for hypersonic vehicles. The rest of this paper is organised as follows. Section 2 presents the calculation model and its theoretical foundations. Three numerical examples of typical parameters used to investigate the polarization properties are presented in Section 3. Finally, Section 4 elaborates the conclusions.

2. Calculation Model and Theoretical Foundations

2.1. Fully Ionised Dusty Plasma Model

The model of complex dielectric parameters under the condition of non-dusty fully ionised plasma collision can be described as follows [10]:

$$\varepsilon_{fe} = 1 + \chi_e + \frac{\sigma_{e1}}{j\omega\varepsilon_0}, \tag{1}$$

where $\omega = 2\pi f$; f represents the incident frequency; $j = \sqrt{-1}$; ε_0 is the permittivity in free space; χ_e denotes the electronic polarisability; and σ_{e1} is the electron–ion collision conductivity. The latter two quantities are derived from the FPL kinetic equation under the long-wavelength approximation:

$$\chi_e = -\frac{\omega_p^2\sqrt{\pi}}{\omega^2}, \qquad \sigma_{e1} = \frac{\sqrt{2}Z_i^2\omega_p^2 e^4 n_i \ln\Lambda}{3\sqrt{\pi m_e}\,\omega^2 (k_B T_e)^{3/2}}, \tag{2}$$

where $\omega_p = \sqrt{n_e e^2 / (\varepsilon_0 m_e)}$ is the plasma frequency; n_e and n_i are the electron number density and ion number density, respectively; e is the electron charge; m_e is the electron mass; Z_i is the ion charge number; $\ln\Lambda$ is the Coulomb logarithm, which is a constant parameter with an approximate range of 10–20 for a typical plasma; k_B is the Boltzmann constant, and T_e is the electron temperature.

When the charging effect is considered, electrons are absorbed after colliding with dust particles within the plasma, and the charging current is found as follows:

$$\begin{aligned} I_{e1} &= -e\int_{v_{\min}}^{\infty} \boldsymbol{v}\cdot\sigma_e^d f_1(v)d\boldsymbol{v} \\ &= \left(-\sigma_e \pi r_d^2 e^{\frac{e\varphi_{d0}}{k_B T_e}} + \sigma_e \pi r_d^2 \frac{2e\varphi_{d0}}{k_B T_e}\Phi_3(u_{\min})\right)\boldsymbol{E} + , \\ & j\frac{8e^2 n_e \pi r_d^2}{3(\pi)^{1/2}\omega m_e}\left(\Phi_1(u_{\min}) - \frac{e\varphi_{d0}}{k_B T_e}\Phi_2(u_{\min})\right)\boldsymbol{E} \end{aligned} \tag{3}$$

where $v_{\min}$ is the minimum incident velocity of the electrons colliding with dust particles; σ_e^d is the collision cross section between the electrons and dust particles; $f_1(v)$ is the perturbed electron distribution function; φ_{d0} is the equilibrium surface potential of the dust particles; and r_d is the radius of the dust particles. $\boldsymbol{v}$ is the electron speed; σ_e is the electron collision conductivity; $\boldsymbol{E}$ is the electric field intensity. The expression of $\Phi_1(u_{\min})$, $\Phi_2(u_{\min})$, and $\Phi_3(u_{\min})$ are as follows:

$$\Phi_1(u_{\min}) = \int_{u_{\min}}^{\infty} u^4 e^{-u^2} du = \frac{1}{2}u^3 e^{-u^2} + \frac{3}{4}ue^{-u^2} + \frac{3\sqrt{\pi}}{8}\left(1-\mathrm{erf}\left(u_{\min}\right)\right), \tag{4}$$

$$\Phi_2(u_{\min}) = \int_{u_{\min}}^{\infty} u^2 e^{-u^2} du = \frac{1}{2}ue^{-u^2} + \frac{\sqrt{\pi}}{4}\left(1-\mathrm{erf}\left(u_{\min}\right)\right) , \tag{5}$$

$$\Phi_3(u_{\min}) = \int_{u_{\min}}^{\infty} u^{-1} e^{-u^2} du = \frac{1}{2}E_i\left(1, u_{\min}^2\right) . \tag{6}$$

here, $u_{\min} = \sqrt{-\frac{e\varphi_{d0}}{k_B T_e}}$

By setting $I_{e1} = \left(\frac{\sigma_{d1}}{\omega^2} + j\frac{\chi_{e1}}{\omega}\right)\boldsymbol{E}$ and substituting the above result into the relation between current density $\boldsymbol{j}_d$ and charging current I_{e1}, the following expression is obtained:

$$\begin{aligned} \boldsymbol{j}_d &= \frac{\omega}{k} n_d \frac{I_{e1}}{j\omega + v_{ch}} \\ &= \frac{\omega}{k} n_d \frac{v_{ch} - j\omega}{\left(\omega^2 + v_{ch}^2\right)} \times \left(\frac{\sigma_{d1} + j\omega\chi_{e1}}{\omega^2}\right)\boldsymbol{E} \quad , \\ &= \frac{\omega}{k} n_d \frac{v_{ch}\sigma_{d1} + \chi_{e1}\omega^2 + j\omega\left(-\sigma_{d1} + \chi_{e1}v_{ch}\right)}{\left(\omega^2 + v_{ch}^2\right)\omega^2}\boldsymbol{E} \end{aligned} \tag{7}$$

where k is the wave number in plasma; n_d is the density of the dust particles; and v_{ch}

represents the electron relaxation rate. σ_{d1} and χ_{e1} are the conductivity and polarisability terms corresponding to the perturbed electron charging current:

$$\sigma_{d1} = -\sigma_{e1}\omega^2\pi r_d^2 e^{\frac{e\varphi_{d0}}{k_B T_e}} + \sigma_{e1}\omega^2\pi r_d^2 \frac{2e\varphi_{d0}}{k_B T_e}\Phi_3(u_{\min}) \quad , \tag{8}$$

$$\chi_{e1} = \frac{8e^2 n_e \pi r_d^2}{3(\pi)^{1/2} m_e}\left(\Phi_1\left(u_{\min}\right) - \frac{e\varphi_{d0}}{k_B T_e}\Phi_2\left(u_{\min}\right)\right) \quad . \tag{9}$$

Ohm's law ($\boldsymbol{j}_d = \sigma_{d\text{complex}}\boldsymbol{E}$, where $\sigma_{d\text{comples}}$ is the complex conductivity related to electron charging) can be used to obtain the complex permittivity, ε_{fd} of the fully ionised plasma under the charging effect:

$$\varepsilon_{fd} = \frac{\omega}{k} n_d \left(\frac{-\sigma_{d1} + \chi_{e1} v_{ch}}{\omega^2\left(\omega^2 + v_{ch}^2\right)\varepsilon_0} + \frac{\sigma_{d1} v_{ch} + \omega^2 \chi_{e1}}{j\omega\varepsilon_0\omega^2\left(\omega^2 + v_{ch}^2\right)}\right) \quad . \tag{10}$$

Finally, combining the collisional and charging effects, the complex permittivities of the two are added as follows: $\varepsilon_{fe} + \varepsilon_{fd}$, which is the total complex permittivity of the fully ionised dusty plasma:

$$\varepsilon_{fe}(\omega) = 1 - \frac{\omega_p^2(\pi)^{1/2}}{\omega^2} + \frac{\omega}{k} n_d \frac{-\sigma_{d1} + \chi_{e1} v_{ch}}{\omega^2\left(\omega^2 + v_{ch}^2\right)\varepsilon_0} + \frac{\sigma_{e1}}{j\omega\varepsilon_0} + \frac{\omega}{k} n_d \frac{\sigma_{d1} v_{ch} + \omega^2 \chi_{e1}}{j\omega\varepsilon_0\omega^2\left(\omega^2 + v_{ch}^2\right)} \quad . \tag{11}$$

2.2. Transmission Line Method

When EM waves with an arbitrary polarization state are incident on a plasma slab at angle θ_0 , an incident wave can be decomposed into perpendicular and parallel polarised waves. A geometric representation of the propagation process is shown in Fig. 1.

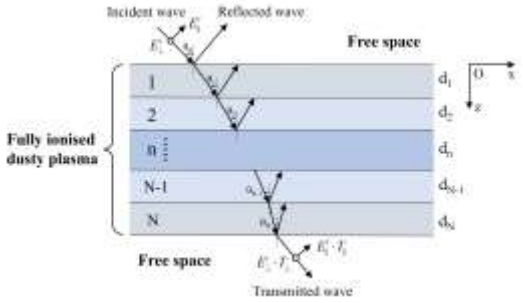


Fig. 1. Schematic diagram of obliquely incident EM wave propagation in fully ionised dusty plasma

As shown in Fig. 1, an incident wave propagated from free space undergoes multiple reflections and refractions inside the plasma layer before the transmitted wave finally enters free space. Inhomogeneous plasma is widely used to divide a medium into several thin layers along the normal propagation direction, with the complex permittivity of each layer approximated as a constant to simplify the solution [19]. The core concept of the transmission line method is to equate the propagation of EM waves along the normal direction of the medium to the transmission of voltage and current on a transmission line [20]. The overall transmission coefficient is solved by cascading the

transmission matrices of each layer [21]. For the *n*th plasma layer, the complex permittivity is determined by both the collisional and charging effects, the specific expressions of which are given in the preceding section. The complex propagation constant of this layer can be expressed as follows:

$$k_n = \omega\sqrt{\mu_0\varepsilon_n} = \beta_n - j\alpha_n, \tag{12}$$

where μ_0 is the permeability of the free space; and β_n and α_n are the phase and attenuation constants of the *n*th layer, respectively.

According to Snell's law, the tangential component of the wave vector is continuous across the interface between the two media [22]:

$$k_0 \sin\theta_0 = k_n \sin\theta_n, \tag{13}$$

where $k_0 = \omega/c$ is the wavenumber in free space; θ_0 is the incident angle in free space; and θ_n is the complex refractive angle of the *n*th plasma layer.

From (13), the normal component of the wave vector in the *n*th layer can be derived as follows:

$$k_{nz} = k_n \cos\theta_n = \sqrt{k_n^2 - k_0^2 \sin^2\theta_0}. \tag{14}$$

In the case of oblique incidence, the perpendicular and parallel polarised waves have different effective characteristic impedances. For the *n*th plasma layer, the effective impedances for the two polarization modes are given as follows:

$$Z_n^{\perp} = Z_n \sec\theta_n, Z_n^{//} = Z_n \cos\theta_n, \tag{15}$$

where $Z_n = \sqrt{\mu_0/\varepsilon_n}$ is the intrinsic characteristic impedance of the *n*th plasma layer and the superscripts $\perp$ and $//$ denote the perpendicular and parallel polarizations, respectively.

For the *n*th plasma layer of thickness d_n, the single-layer transmission matrix along the normal direction takes the following form:

$$\begin{bmatrix} A_n^{\perp} & B_n^{\perp} \\ C_n^{\perp} & D_n^{\perp} \end{bmatrix} = \begin{bmatrix} \cosh(jk_{nz}d_n) & Z_n^{\perp}\sinh(jk_{nz}d_n) \\ \sinh(jk_{nz}d_n)/Z_n^{\perp} & \cosh(jk_{nz}d_n) \end{bmatrix}, \tag{16}$$

$$\begin{bmatrix} A_n^{//} & B_n^{//} \\ C_n^{//} & D_n^{//} \end{bmatrix} = \begin{bmatrix} \cosh(jk_{nz}d_n) & Z_n^{//}\sinh(jk_{nz}d_n) \\ \sinh(jk_{nz}d_n)/Z_n^{//} & \cosh(jk_{nz}d_n) \end{bmatrix}. \tag{17}$$

For a nonuniform plasma structure consisting of *N* layers, the overall transmission matrices for the two polarization modes can be obtained by cascading the single-layer transmission matrices in the order of wave propagation [23]:

$$\begin{bmatrix} A^{\perp} & B^{\perp} \\ C^{\perp} & D^{\perp} \end{bmatrix} = \begin{bmatrix} A_1^{\perp} & B_1^{\perp} \\ C_1^{\perp} & D_1^{\perp} \end{bmatrix}\begin{bmatrix} A_2^{\perp} & B_2^{\perp} \\ C_2^{\perp} & D_2^{\perp} \end{bmatrix}\cdots\begin{bmatrix} A_N^{\perp} & B_N^{\perp} \\ C_N^{\perp} & D_N^{\perp} \end{bmatrix}, \tag{18}$$

$$\begin{bmatrix} A^{//} & B^{//} \\ C^{//} & D^{//} \end{bmatrix} = \begin{bmatrix} A_1^{//} & B_1^{//} \\ C_1^{//} & D_1^{//} \end{bmatrix}\begin{bmatrix} A_2^{//} & B_2^{//} \\ C_2^{//} & D_2^{//} \end{bmatrix}\cdots\begin{bmatrix} A_N^{//} & B_N^{//} \\ C_N^{//} & D_N^{//} \end{bmatrix}. \tag{19}$$

The lateral shift of the transmitted wave introduces a phase factor:

$$P^t = \exp\left(-jk_0 \sin\theta_0 \sum_{n=1}^{N} d_n \tan\theta_n^t\right), \tag{20}$$

where θ_n^t denotes the actual refractive angle of the *n*th layer. The total transmission coefficients for the two polarizations are as follows:

$$T_{\perp} = \frac{2}{\left(A^{\perp} + B^{\perp}/Z_{N+1}^{\perp}\right) + Z_0^{\perp}\left(C^{\perp} + D^{\perp}/Z_{N+1}^{\perp}\right)} P^t, \tag{21}$$

$$T_{//} = \frac{2}{\left(A^{//} + B^{//} / Z_{N+1}^{//}\right) + Z_0^{//}\left(C^{//} + D^{//} / Z_{N+1}^{//}\right)} P^t . \tag{22}$$

where $Z_0^{\perp} = Z_0 \sec\theta_0, Z_0^{//} = Z_0 \cos\theta_0$ are the effective impedances of free space for the two polarizations, and $Z_0 = \sqrt{\mu_0 / \varepsilon_0}$.

2.3. Polarization Property

For EM waves with an arbitrary polarization state obliquely incident on the plasma, the transmitted wave can be recombined using the parallel and perpendicular polarization components:

$$\boldsymbol{E}^t = E_{//}^i T_{//} \mathbf{u}_{//} + E_{\perp}^i T_{\perp} \mathbf{u}_{\perp}, \tag{23}$$

where $E_{//}^i$ and $E_{\perp}^i$ are the amplitudes of the incident parallel and perpendicular polarised components, respectively; $T_{//}$ and $T_{\perp}$ are the complex transmission coefficients for the parallel and perpendicular polarizations, respectively; and $\mathbf{u}_{//}$ and $\mathbf{u}_{\perp}$ are the unit vectors along the parallel and perpendicular polarization directions, respectively.

The phase difference between the Transverse Electric (TE) and Transverse Magnetic (TM) components of the transmitted wave is defined as follows:

$$\begin{aligned} \varphi^t &= \varphi_{\perp}^t - \varphi_{//}^t \\ &= \arg(E_{\perp}^i T_{\perp}) - \arg(E_{//}^i T_{//}) \pm 90^{\circ} \end{aligned}, \tag{24}$$

where $\varphi_{\perp}^t$ and $\varphi_{//}^t$ represent the phases of the perpendicular and parallel polarised waves of the transmitted wave, respectively. The sign of the phase difference determines whether the transmitted wave is left-handed or right-handed polarised. According to the polarization theory of EM waves, the axial ratio can be calculated as follows [24]:

$$AR = \tan\left(\frac{1}{2}\arcsin\left(\frac{2\left|E_{//}^i T_{//}\right|\left|E_{\perp}^i T_{\perp}\right|\sin\phi^t}{\left|E_{//}^i T_{//}\right|^2 + \left|E_{\perp}^i T_{\perp}\right|^2}\right)\right). \tag{25}$$

According to the general convention in polarization theory, the axial ratio characterises the polarization state of the transmitted wave. Generally, decibel (dB) is used to describe the magnitude of the axial ratio:

$$AR(\mathrm{dB}) = 20\log_{10}(AR) \tag{26}$$

A value of zero corresponds to ideal circular polarization, an infinite value indicates linear polarization, and other values denote elliptical polarization.

A differential polarization state between the incident and transmitted waves can induce a polarization mismatch between the transmitted signal and receiving antenna. The Stokes parameters are useful for fully describing the transmitted wave. The Stokes parameters of a transmitted wave are defined as follows:

$$\begin{cases} g_0^t = \left|E_{//}^i T_{//}\right|^2 + \left|E_{\perp}^i T_{\perp}\right|^2 \\ g_1^t = \left|E_{//}^i T_{//}\right|^2 - \left|E_{\perp}^i T_{\perp}\right|^2 \\ g_2^t = 2\left|E_{//}^i T_{//}\right|\left|E_{\perp}^i T_{\perp}\right|\cos\phi^t \\ g_3^t = 2\left|E_{//}^i T_{//}\right|\left|E_{\perp}^i T_{\perp}\right|\sin\phi^t \end{cases}. \tag{27}$$

Assuming the receiving antenna is an ideal RHCP antenna with Stokes parameters

denoted as $[g_0^r, g_1^r, g_2^r, g_3^r]$, the polarization matching coefficient between the received signal and receiving antenna is given by the following:

$$m_p = \frac{g_0^t g_0^r + g_1^t g_1^r + g_2^t g_2^r + g_3^t g_3^r}{2 g_0^t g_0^r} . \tag{28}$$

The polarization mismatch loss is defined as the decibel form of the matching coefficient:

$$\text{Loss} = 10\lg(m_p)\text{dB} . \tag{29}$$

This parameter directly reflects the received power loss caused by the polarization mismatch. A smaller value indicates a more severe mismatch and less signal power available to the receiving antenna.

3. Results and Discussion

We analysed the effects of fully ionised dusty plasma on the polarization properties of RHCP waves received by an RHCP antenna. The effects of the dust radius, dust density, and X-band incident wave frequency on the axial ratio, phase difference, and polarization mismatch loss of the transmitted waves were investigated in detail.

3.1. Validity Analysis

To verify the accuracy of our numerical results, we compared them to those from a previous study [17]. The calculation parameters were consistent. Specifically, the peak electron density of the plasma sheath was $5\times10^{17}\text{m}^{-3}$; the plasma collision frequency was 1GHz; the incident wave was a GPS L1-band RHCP wave; and the scanning range of the incident angle was $0^\circ - 90^\circ$.

In Fig. 2, the solid red line represents the results obtained by the theoretical analysis method in the previous study, and the solid black line denotes the axial ratio curve calculated in this study. The two curves are in excellent agreement over the entire scanning range, which verifies the accuracy of the transmission line analogy method and calculation procedure for the polarization parameters. Therefore, it is feasible to introduce a complex permittivity model for fully ionised dusty plasma.

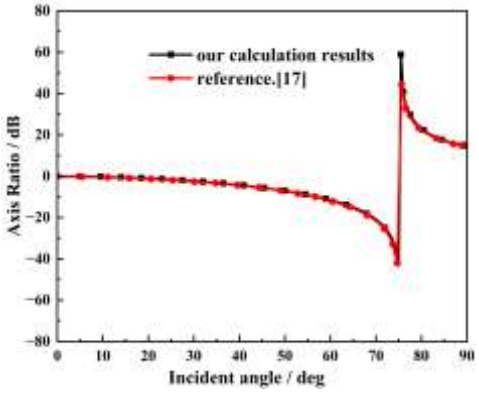


Fig. 2. Comparison of axial ratio calculation results

After the above validation, the effects of the dust radius, dust density, and X-band incident frequency on the polarization properties of obliquely incident electromagnetic waves under fully ionised dusty plasma were systematically analysed; the calculation parameters are summarised in Table 1. All of the parameter values were referenced from a typical flow field for the stagnation region of hypersonic reentry vehicles. The electron density and temperature fell within the typical ranges for fully ionised reentry plasma sheaths, and their orders of magnitude were consistent with those of similar studies based on the FPL collision model [10]. The values of the dust radius and density

covered the typical size and density ranges of ablated particles from vehicle thermal protection materials [25]. The X-band is one of the core frequency bands employed for the tracking, telemetry, and command communication of reentry vehicles. Thus, it was selected as the research frequency band. Compared to the lower bands, the X-band exhibits a significantly stronger penetration capability through the plasma sheath, as verified by early flight experiments and theoretical analyses [26,27]. Consequently, it remains the preferred band for blackout mitigation in contemporary studies [3,28].

Table 1. Calculation parameters in Figures 3–5.

	r_d (μm)	n_d (m^{-3})	f (GHz)
Fig. 3	2,4,5,7	2×10^{14}	10
Fig. 4	2	2×10^{14}, 4×10^{14}, 5×10^{14}, 6×10^{14}	10
Fig. 5	2	2×10^{14}	8,9,10,11

The following common parameters were used: electron density n_e=$1\times10^{19}m^{-3}$, electron temperature T_e=10000K, ion mass m_i=6×10^{-26}kg, ion charge state Z_i=1, $\ln\Lambda = 20$, and total thickness of the plasma slab L=0.05m.

3.2. Effect of Dust Radius

This section discusses the results when the dust density was fixed at $2\times10^{14}m^{-3}$ and the incident wave frequency was fixed at 10GHz. Four dust radius values were selected for comparative analysis: 2μm, 4μm, 5μm, and 7μm. Fig. 3 shows the axial ratio, phase difference, and polarization mismatch loss values of the transmitted wave when using different values for the dust radius.

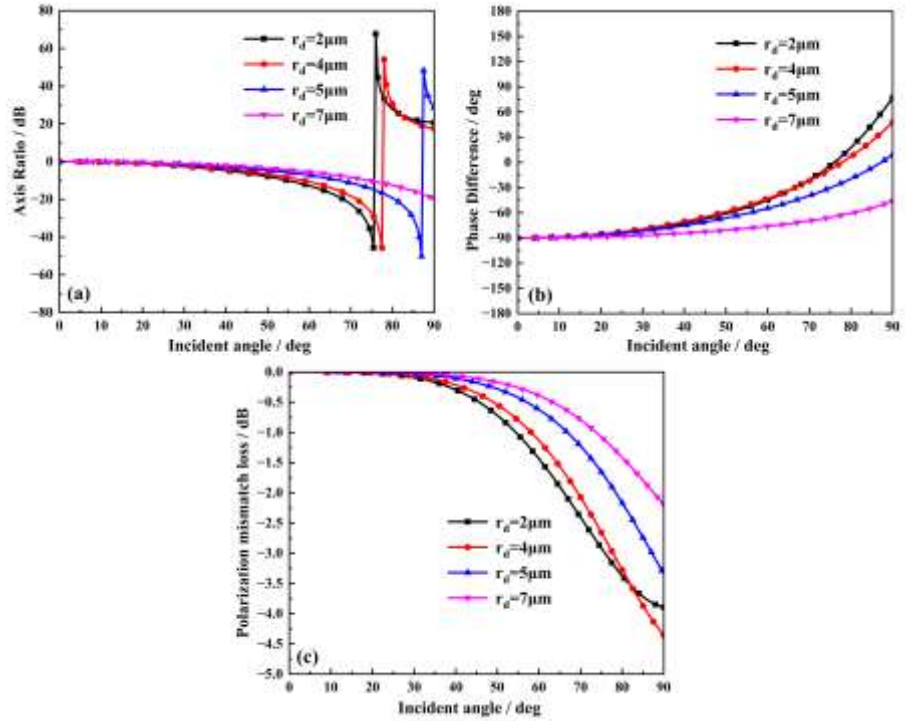


Fig. 3. Effects of different values of dust radius on the polarization properties of EM waves. (a) axial ratio, (b) phase difference, and (c) polarization mismatch loss

The results indicated that for all four dust radius values, the axial ratio generally increased with the incident angle. The polarization mismatch loss increased accordingly, and the TE-TM phase difference gradually deviated from −90°. In addition, polarization

reversal from RHCP to LHCP occurred over a large incident angle range. For a given incident angle, a smaller dust radius led to a larger absolute axial ratio, higher polarization mismatch loss, and smaller critical angle for polarization reversal.

As shown in Fig. 3(a), the critical angle for polarization reversal was approximately 75.5° when the dust radius was 2μm. The critical angle gradually increased with the radius. Specifically, when the radius increased to 5μm, the critical angle of polarization reversal increased by approximately 13°. When the radius reached 7μm, the axial ratio remained negative across the entire range of incident angles, and no polarization reversal occurred. The phase difference curves in Fig. 3(b) show that the TE-TM phase difference remained stable around −90° at small incident angles and gradually shifted toward positive values as the angle increased. Notably, the zero-crossing point of the phase difference corresponded to the critical angle of axial ratio reversal. Moreover, with a smaller dust radius, the phase difference shifted more rapidly with the incident angle. Regarding the polarization mismatch loss shown in Fig. 3(c), considering an incident angle of 70° as an example, the loss was approximately −2.4dB for a dust radius of 2μm and −0.8dB for a dust radius of 7μm, resulting in a difference of approximately 1.6dB between the two cases.

Overall, an appropriate increase in the dust radius could effectively mitigate the polarization deterioration of obliquely incident EM waves, increase the critical angle of polarization reversal, and decrease the polarization mismatch loss. These findings indicated that the dust radius significantly influences the polarization properties.

3.3. Effect of Dust Density

The dust radius was fixed at $2\,\mu m$, and the other common parameters remained the same as those described in Section 3.2. Four dust density values were selected for comparative analysis: $2\times10^{14}m^{-3}$, $4\times10^{14}m^{-3}$, $5\times10^{14}m^{-3}$, and $6\times10^{14}m^{-3}$. The corresponding results are shown in Fig. 4.

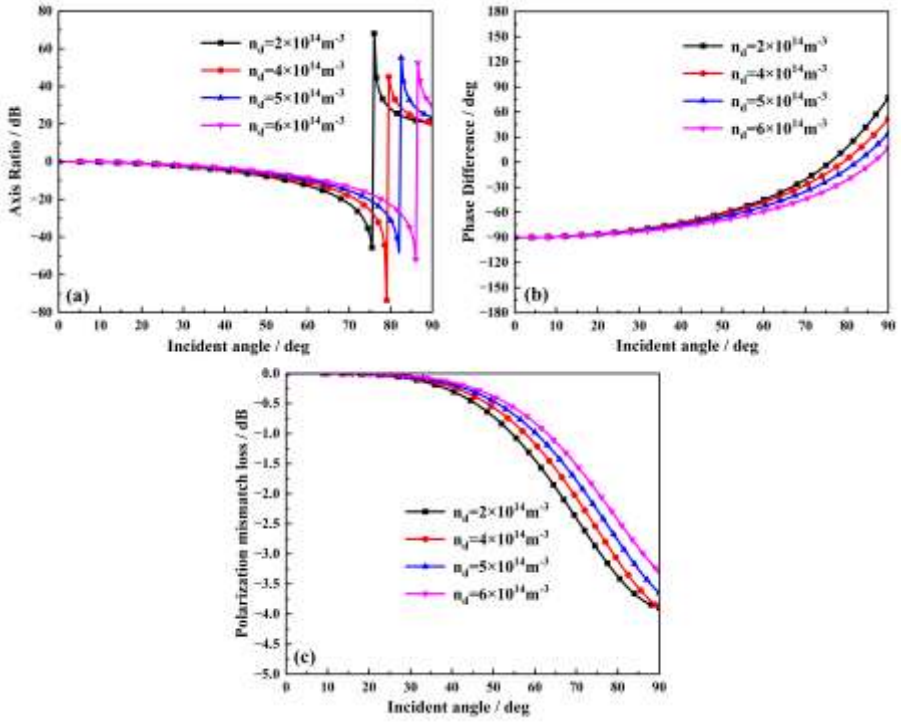


Fig. 4. Effects of different values of dust density on the polarization properties of EM waves: (a) axial ratio, (b) phase difference, and (c) polarization mismatch loss.

Similar to the influence of the dust radius, the axial ratio and polarization mismatch loss both increased with the incident angle for all four values of dust density. The TE-TM phase difference gradually deviated from −90°, and polarization reversal occurred over a large incident-angle range. At a fixed incident angle, a lower dust density resulted in a larger absolute axial ratio, higher polarization mismatch loss, and smaller critical angle for polarization reversal, implying more severe polarization deterioration.

As shown in Fig. 4(a), the critical angles of polarization reversal for the four dust density groups were approximately 75.5°, 79°, 82°, and 86°. The critical angle increased with the dust density. The phase difference curves in Fig. 4(b) indicate that the zero-crossing position of the phase difference corresponded to the critical angle of axial ratio reversal. Moreover, with a lower dust density, the phase difference shifted more rapidly with the incident angle. For the polarization mismatch loss in Fig. 4(c), considering an incident angle of 70°as an example, the loss was approximately −2.4dB for the lowest dust density group and approximately −1.5dB for the highest density group. When the dust density tripled, the polarization mismatch loss decreased by approximately 0.9dB.

An appropriate increase in dust density could mitigate polarization deterioration; however, its overall effect was weaker than that of the dust radius.

3.4. Effect of Incident Wave Frequency

The dust radius was fixed at 2μm, and the density was fixed at $2\times10^{14}m^{-3}$. Four values of incident frequency in the X-band were selected for calculation: 8GHz, 9GHz, 10GHz, and 11GHz, and the results are shown in Fig. 5.

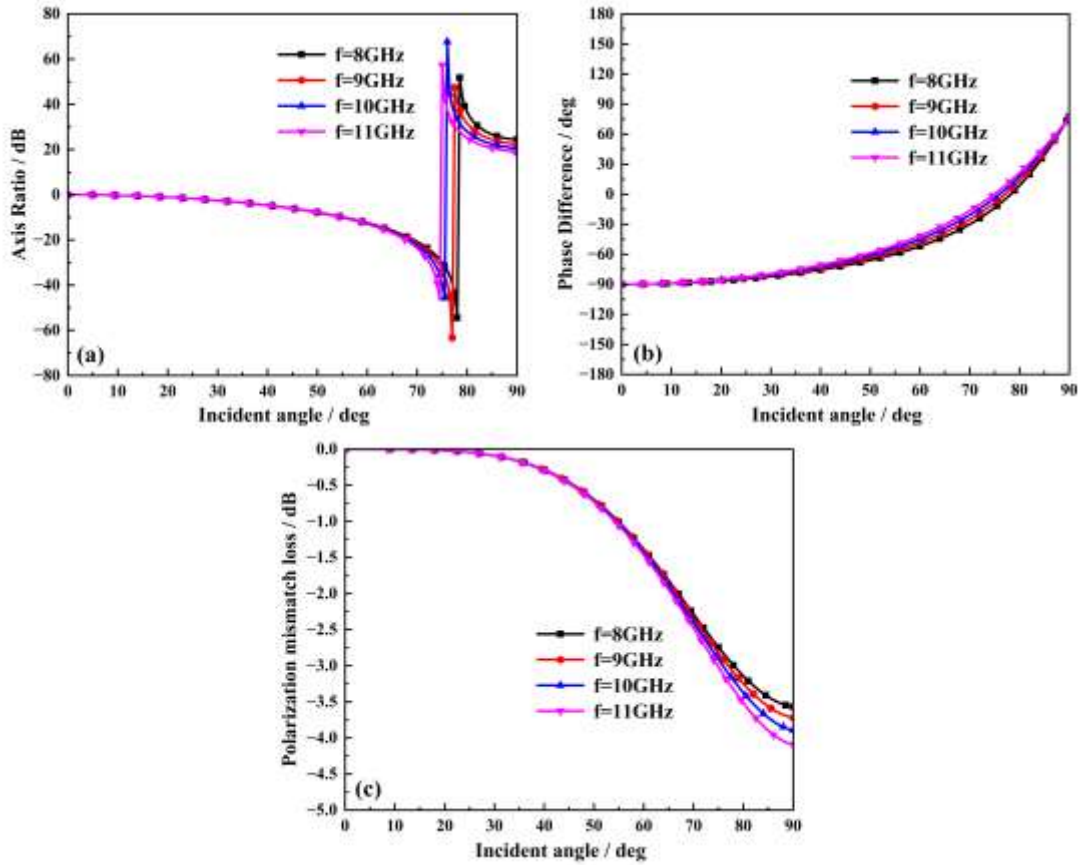


Fig. 5. Effects of different incident wave frequencies in X band on the polarization properties of EM waves. (a) axial ratio, (b) phase difference, and (c) polarization mismatch loss

The calculation results indicated that for all four incident frequency values, both

the axial ratio and polarization mismatch loss increased with the incident angle. The TE-TM phase difference deviated progressively from -90°, and polarization reversal occurred over a large incident-angle range. This overall trend was consistent with those observed for the dust radius and density cases. Within the X-band, a higher incident frequency led to a larger absolute axial ratio and higher polarization mismatch loss at the same incident angle, indicating more severe polarization deterioration.

As shown in Fig. 5(a), the critical angles of polarization reversal for 8GHz and 11GHz differed by approximately 4°, and a higher frequency led to a slight decrease in the critical angle. The phase difference results in Fig. 5(b) indicate that the phase difference shifted from -90° toward positive values with an increase in the incident angle for all frequency groups. At the same incident angle, a higher incident frequency led to a larger phase-difference shift and smaller zero-crossing critical angle. This variation trend in the phase difference was consistent with the variation pattern of the axial ratio. As shown in Fig. 5(c), considering an incident angle of -70°as an example, the polarization mismatch loss was approximately −2.3dB at 8GHz and approximately −2.3dB at 11GHz, indicating a minor difference between the two cases.

Overall, an increase in the operating frequency within the X-band slightly aggravated the polarization deterioration of the obliquely incident waves. However, its influence was weaker than those of the dust radius and dust density.

4. Conclusion

In this study, a complex permittivity model for fully ionised dusty plasma was established based on the FPL collision model and OML theory. The transmission line analogy method was adopted to calculate the transmission characteristics of obliquely incident EM waves. On this basis, the effects of the dust radius, dust density, and X-band incident frequency on the polarization properties of transmitted waves were quantitatively analysed.

The main conclusions are summarised as follows. An increase in the incident angle was the dominant factor causing polarization deterioration. As the incident angle increased, the axial ratio showed an overall upward trend, the phase difference between the TE and TM components continuously deviated from -90°, polarization reversal from RHCP to LHCP occurred at large incident angles, and the polarization mismatch loss increased correspondingly. Within the X-band, a higher incident frequency aggravated polarization deterioration; however, its impact was weaker than those of the dust radius and density under the parameter range adopted in this study. Significantly, dust particles do not always degrade communication performance. A moderate increase in the dust radius or density can reduce the transmission discrepancy between the TE and TM components, increase the critical angle for polarization reversal, and lower the polarization mismatch loss. The influence of dust radius was found to be more pronounced than that of dust density. These results provide a theoretical basis for the polarization matching design of hypersonic vehicle reentry communication links and for alleviating the communication blackout issue.

Acknowledgment

This work was supported in part by the National Natural Science Foundation of China (Grant Nos.62501230, 62231021, U25A20412). Natural Science Foundation of Henan Province (Grant Nos. 252300423327, 262300420670), Henan Provincial Science and Technology Research Project (Grant Nos. 252102210194, 262102210034). We would like to thank Editage (www.editage.cn) for English language editing.

References

[1] Vpland D, Randall T, Lawrence D, McClinton, Charles R 2006 *Acta Astronaut.* **59** 181
[2] Rybak J P and Churchill R J 1971 *IEEE Trans. Aerosp. Electron. Syst.* AES-7 879
[3] Zhong W B, Zhao Z Y, Yuan K and Tang R X 2025 *Phys. Plasmas* **32** 073504
[4] Deng Q Q, Chen C X, Chen W, Yang L X, Hu X Q, Ye S Y, Huang Z X, Guo L X, Ye Y 2023 *IEEE Trans. Plasma Sci.* 2023 **51** 847
[5] Wang Z Y, Yin H C, Guan L, Dang X W, Deng H C and Tan Z P 2025 *IEEE Trans. Plasma Sci.* **53** 806
[6] Li X and Jing Z 2025 *Phys. Plasmas* **32** 083703
[7] Chen W, Wang Z Y, Yang L X, Huang Z X, Guo L X Wang L F 2021 *IEEE Trans. Plasma Sci.* **49** 1460
[8] Jia J S, Yuan C X, Liu S, Yue F, Gao R L, Wang Y, Zhou Z X, Wu J and Li H 2016 *Phys. Plasmas* **23** 043302
[9] Liu Y T, Chen W, Yang L X, Huang Z X, Guo L X, Guo L J and Deng Q Q 2020 *Phys. Plasmas* **27** 093702
[10] Li D, Guo L X and Li J T 2018 *Phys. Plasmas* **25** 013707
[11] Guerra R and Mendonça J T 2000 *Phys.Rev. E* **62** 1190
[12] Chen W, Huang H, Yang L X, Bo Y and Huang Z X 2023 *Acta Phys. Sin.* **72** 060201
[13] Luc A, Pascaud R, Mazières V, Simon A, Loridan V, Mazé-Merceur G, Girard M, Laquerbe V, Monchaux D, Romero T, Pouliguen P, Lunaud G and Callegari T 2026 *Phys. Plasmas* **33** 032102
[14] Liu Z W, Bao W M, Li X P, Liu D L and Bai B W 2015 *IEEE Trans. Plasma Sci* **43** 3147
[15] Bai B W, Liu Y M, Li X P, Yao B and Shi L 2018 *Phys. Plasmas* **25** 062101
[16] Shahrokhi A, Mehdian H, Hajisharifi K and Hasanbeigi A 2017 *Appl. Phys. B* **123** 292
[17] Bai B W, Li X P, Liu Y M, Xu J, Shi L and Xie K 2014 *IEEE Trans. Plasma Sci* **42** 3365
[18] Gan L P, Guo L X, Li J T and Guo L J 2021 *Int. J. Antennas Propag.* **2021** 2630979
[19] Deng Q Q, Chen C X, Chen W, Yang L X, Hu X Q and Ye S Y 2023 *IEEE Trans. Plasma Sci* **51** 847
[20] A. S. Bronwell, 1944 *Proceedings of the IRE* **32** 233-241
[21] Y. Wang, H. Zhang, Q. Zhao, and Y. Li 2019 *AIP Adv.* **9** 085305
[22] Zhang Q C, Tian Z Y, Tang W Y, Tang N, Zhao H and Lin H 2019 *J. Appl. Phys.* **125** 094902
[23] Savino R, D'Elia M E and Carandente V 2015 *J. Spacecr. Rockets* **52** 417
[24] S. R. Clodue 1983 *Microwave J* **26** 119-127
[25] Habeck J B, Kroells M D, Schwartzentruber T E and Candler G V 2024 *AIAA Journal* **62** 460
[26] Akey N D and Cross A E 1970 Radio Blackout Alleviation and Plasma Diagnostic (Washington D.C.: National Aeronautics and Space Administration) NASA TN D-5615
[27] Langley Research Center 1970 *The Entry Plasma Sheath and Its Effects on Space Vehicle Electromagnetic Systems,* Volume 1*,* October 13-15, 1970, Hampton, Virginia, NASA SP-252
[28] Shi L, Liu Z Y, Bao W M, Yao B, Wang Y F, Li X P, Liu Y M and Li F Y 2024 *Chin. J. Aeronaut.* **37** 26